DOI: 10.21062/mft.2023.086 http://www.journalmt.com

Austenitic Steel AISI 304 under Static and Cyclic Loading

Veronika Chvalníková (0009-0002-1523-8065), Milan Uhríčik (0000-0002-2782-5876), Peter Palček (0000-0001-7902-2007), Martin Slezák (0009-0008-3181-0862), Lukáš Šikyňa (0900-0004-7168-6852), Petra Drimalová (0000-0001-8461-9529)
Faculty of Mechanical Engineering, Department of Materials Engineering, University of Žilina, Univerzitná 8215/1, 010 26 Žilina. Slovakia. E-mail: veronika.chvalnikova@fstroj.uniza.sk, milan.uhricik@fstroj.uniza.sk, peter.palcek@fstroj.uniza.sk, martin.slezak@fstroj.uniza.sk, lukas.sikyna@fstroj.uniza.sk, petra.drimalova@fstroj.uniza.sk.

The paper is aimed at establishing knowledge of the failure mechanisms and plastic behaviour of austenitic steel AISI 304 in the initial state under different loading conditions. Microstructural analysis was performed on a light microscope Neophot 32. AISI 304 austenitic steel has a microstructure formed by a large number of polyhedral austenite grains of different sizes. The steel microstructure, mechanical and fatigue properties, and areas of the plastic zone after the bending impact test were investigated. The surface hardness of samples was measured on a Zwick Roell ZHVμ microhardness measuring device using the Vickers method. After the bending impact test, fractures were formed with significant deformation with a typical pit morphology. The fatigue test, performed on a Zwick Roell resonant pulsator, monitored the plastic deformation causing changes in mechanical properties. Finally, fractographic evaluations of the fracture surfaces were performed on a Tescan Vega LMUII scanning electron microscope. The result of the work will demonstrate the differences in material behaviour under both static and cyclic loading.

Keywords: Austenitic steel, Crack, Fracture, Static loading, Cyclic loading

1 Introduction

Structural steels with a high additive content usually have very good mechanical, chemical, and physical properties. Stainless steels are steels with increased resistance to aggressive environments. Austenitic steels are mostly used for industrial, transportation, and domestic products such as handling service equipment, seat belt anchors, exhausts, pots, sinks, brewing equipment, and many others. Due to their long service life, good maintenance, or simplicity of welding, they are partly used in the nuclear power industry, petrochemical, pharmaceutical, or paper industries [1-3]. Disadvantages include poorer machinability and high price, a tendency to corrosion cracking under stress, but also poor thermal conductivity caused by a relatively large number of alloying elements. For several types of stainless steels, chromium is the basic alloying element, which slows down corrosion with increasing content, i.e. makes the steel passive against corrosion. Passivation means the formation of thin oxide surface layers that are the result of reactions with the surrounding environment. The ability to passivate the material is the essence of corrosion resistance, which leads to the slowing down of chemical and electrochemical reactions [4,5]. Another important alloying element is nickel, which is electrochemically noble, supports the formation of oxide layers, increases resistance to reducing acids, and positively affects the mechanical properties of the material. Other alloying elements such as manganese, molybdenum, and silicon must be properly balanced to achieve the desired austenitic structure. By adjusting the carbon content or alloying elements, it is possible to increase the overall corrosion resistance, corrosion cracking resistance, mechanical properties, machinability, or weld cracking resistance. In general, these steels are well-formable and can be stable even at low temperatures or strong at high temperatures. Care must be taken to ensure proper heating during hot forming or heat treatment because steels have poorer thermal conductivity at lower temperatures. If the corrosion-resistant steel is heated very quickly, it could crack due to high stresses. These stresses would be created by differential temperatures between the surface and the core. Austenitic steels can withstand faster heating compared to martensitic steels. At a temperature of 900 °C, they have the same thermal conductivity, which increases with elevated temperature. At the end of heating, too slow temperature increase, too long heating at final temperatures, and also overheating of the steel is undesirable, because as soon as all carbides are dissolved, the grain begins to coarsen [6-9].

Fatigue is the most common source of failure in mechanical structures. Fatigue begins during a large number of cycles when damage develops at the microplastic level and grows until a macroscopic crack occurs. It grows with each subsequent cycle until it reaches a critical length and the component breaks because it cannot sustain the accumulated stress and load. In some applications, crack propagation stops or grows so fast that component failure occurs earlier. A loading cycle is defined as the duration from one peak of the observed variable to the next peak. The stress varies between the maximum and minimum stress during the load cycle [10-15]. The Wöhler curve is the most classic characteristic of high-cycle fatigue. It is used to determine when a brittle fracture will occur under a given load. It is plotted in logarithmic coordinates, where the load amplitude and the number of cycles to fracture are plotted. To create it, it is necessary to do a load experiment for different levels. The fatigue process involves two phases, crack initiation, and crack propagation. Some important load-bearing structural components may fail prematurely in service. This is due to manufacturing defects and imperfections such as forging defects, inclusions caused by welding, surface scratches, corrosion pits, and others, which lead to the formation of surface cracks or internal defects that propagate into sudden failure [16-18].

2 Experimental part

The AISI 304 austenitic stainless steel used as the experimental material was supplied as 3 m square-base bars with dimensions of 10x10 mm and specimens of the required length of 55 mm were cut from it. The cutting of specimens was carried out on a Proma band saw type PPK-155. After cutting, V-grooves with an angle of 45° and a depth of 2 mm were milled into specimens according to STN EN 10045-1 standard on a universal milling cutter UWF 200. The chemical composition of the stainless steel was determined on a SPECTROMAXx spark emission spectrometer. The measured values are listed in Tab. 1, together with values from the STN 17 240 standard.

Tab. 9 *Chemical composition of the austenitic stainless steel (in wt. %)*

	C	Mn	Si	Cr	Ni	Mo	S	P	Fe
AISI 304	0.03	1.44	0.31	18.87	7.8	0.24	0.04	0.02	balance
STN 17240	≤0.07	≤ 2	≤ 1	17.0-20.0	9.0-11.5	-	0.03	0.045	balance

The microhardness of specimens was measured by the Vickers method on a Zwick Roel ZHVμ micro-hardness measuring device. During the test, a diamond quadrilateral pyramid with an apex angle of 136° is pressed into the specimens with a selected load of 0.5 kp. The hardness curve was measured from one edge to the core with loading for 10 seconds for one press, at a temperature of 20°C.

The bending impact test was carried out on a pendulum hammer (Charpy). The test procedure is implemented according to the EN 10045-1 standard.

A Fatigue test was performed on a Zwick Roell-Amsler 150 HFP 5100 resonance pulsator. Multiple cyclic plastic deformation during fatigue loads causes changes in the material when the mechanical properties change and the final failure of the material by fatigue fracture occurs.

The Tescan Vega LMUII scanning electron microscope was used to perform fractographic evaluations of fracture surfaces after bending impact tests and after Fatigue tests, as well as observation of specimen surfaces after tests in which plastic zone propagations were observed. EDX analysis, which is part of the scanning electron microscope, was used to determine, verify and detect phases that are present in the structure.

3 Results and discussion

Austenitic steel AISI 304 has a microstructure formed by a large number of polyhedral austenitic grains of different sizes (Fig. 1). As a result of the processing of the material (technological processing at the manufacturer), annealing twins and deformation martensite were found in the structure. The deformation martensite was formed as a result of rolling, and the annealing twins were formed due to the increased temperature during rolling.

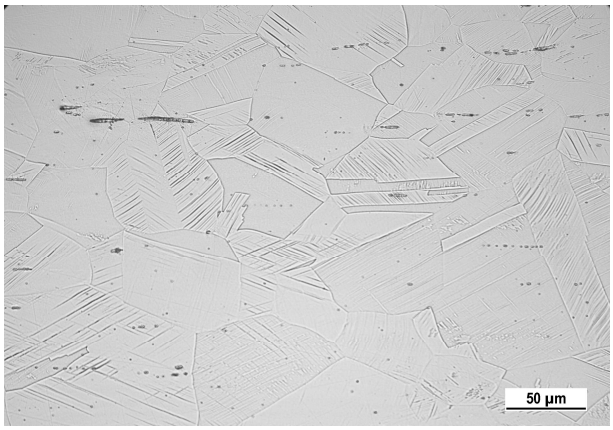

Fig. 19 *Microstructure of AISI 304 austenitic steel, etched. glycerol+hydrofluoric acid+nitric acid*

The microstructure contains non-metallic inclusions such as manganese sulphides and oxides based on aluminum and silicon. Evidence of their presence is shown in Fig. 2 and Fig. 3.

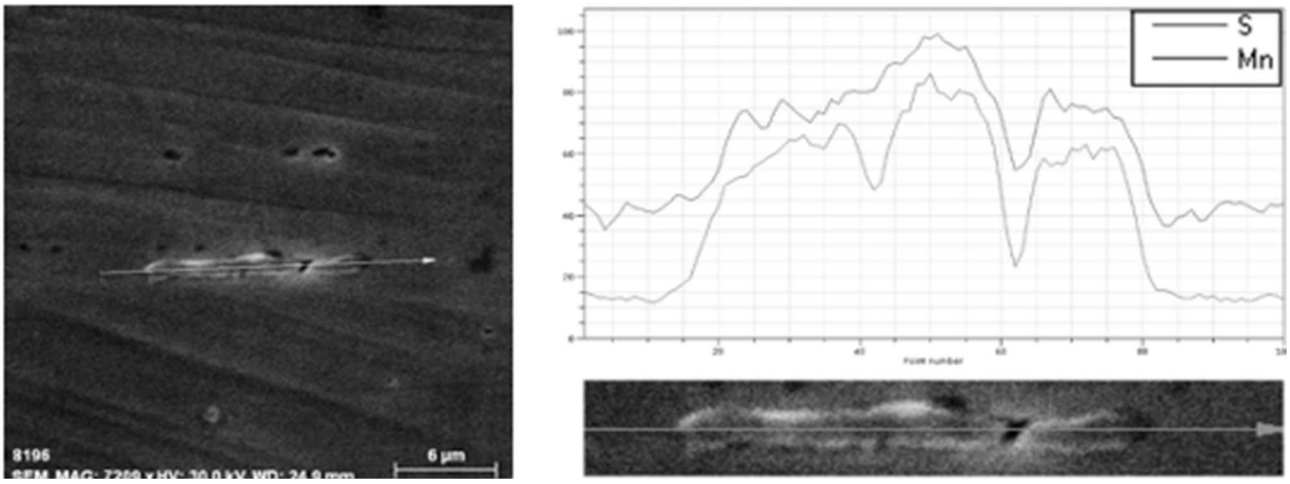

Fig. 20 *Verification of manganese sulfide by EDX analysis – line-scan*

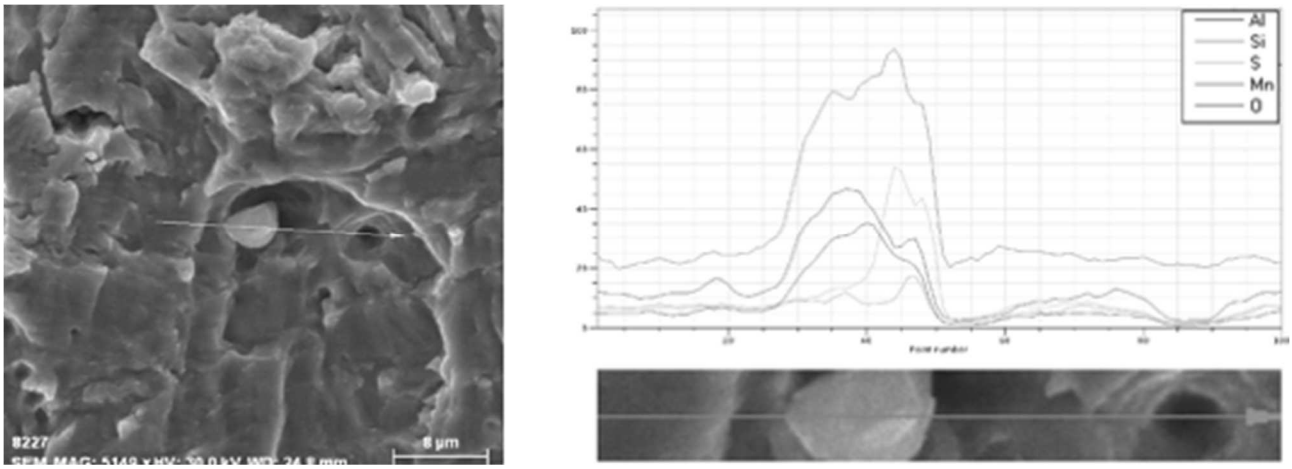

Fig. 21 *Verification of Al- and Si-based oxides by EDX analysis – line-scan*

The average measured microhardness value of the experimental material AISI 304 was 294 HV 0.5. The minimum measured microhardness value was 251 HV 0.5 and the maximum measured value was 337 HV 0.5. The course of microhardness of austenitic steel AISI 304 is shown in Fig. 4.

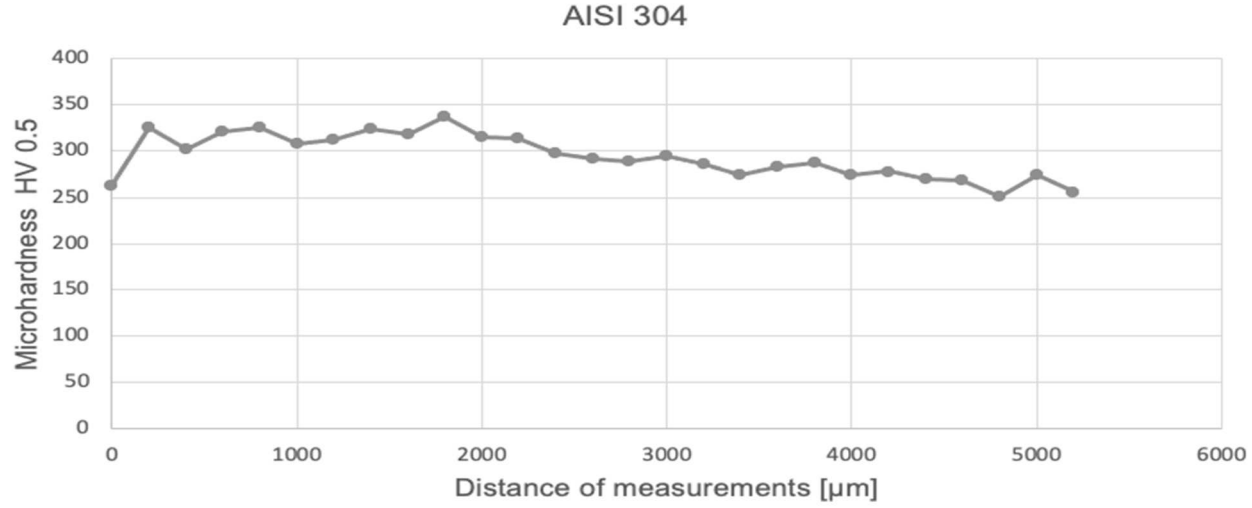

Fig. 22 *Course of microhardness of AISI 304 austenitic steel*

During the bending impact test on a Charpy hammer, the resistance of AISI 304 austenitic steel to puncture was observed, as well as the fracture and the surface character of the specimen after this dynamic test. The average value of absorbed energy after breaking through specimens was 123.2 J.

Before the bending impact test, the specimen surfaces were metallographically prepared and observed with a scanning electron microscope (SEM). Fig. 5 shows the microstructure of AISI 304 austenitic steel before the bending impact test, where we observe the structure created during the processing of the material (annealing twins and also the deformation martensite). Subsequently, a dynamic test was performed on a Charpy hammer, and after the test, these surfaces, as well as the fractures themselves, were observed on SEM.

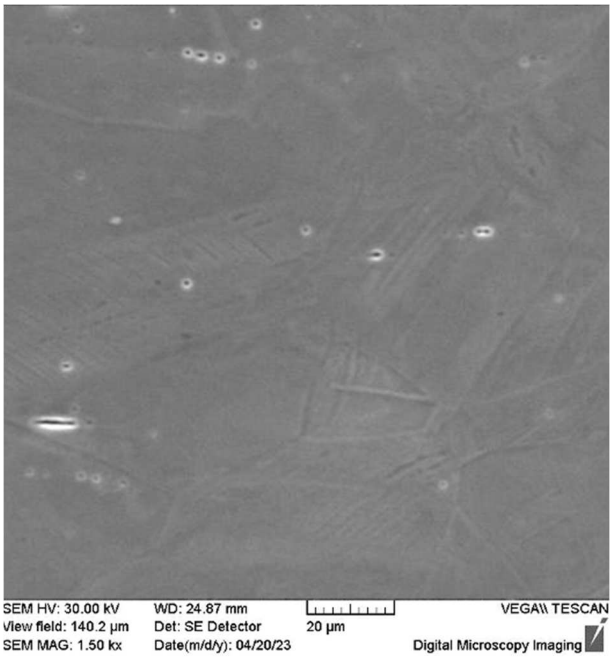

Fig. 23 *The surface of the AISI 304 specimen before the bending impact test, etched. Kalling's II*

After the bending impact test, a plastic area was observed on the punctured specimens around the notch (Fig. 6), respectively in the places near cracks. Most commonly, plastic deformation was manifested by slip dislocations. Plastically deformed annealing twins were also clearly visible, with significantly thicker slip bands.

Using fractography, the character of failure and ductility can be analyzed. The test specimens failed by ductile fracture with a typical pit morphology (Fig. 7). Deep pits were observed on the fracture surface. Sulfide and oxide particles were observed at the bottom of the pits, which create the so-called textured fracture, and due to them the rolling direction, linearity, and deformation texture can be observed.

Fatigue tests (by three-point cyclic bending) were performed on a frequency pulsator in the range of the number of cycles $N_f \approx 10^4$ to $N_f \approx 2x10^7$. The loads applied to samples are the mean stress σ_m = -270 MPa and the stress amplitude σ_a = 45 - 180 MPa. From the results of dynamic fatigue tests, a Wöhler curve (S-N curve) was constructed, showing the dependence of the upper-stress σ_h on the number of cycles to failure N_f (Fig. 10). Samples that lasted $2x10^7$ cycles are considered "run-outs".

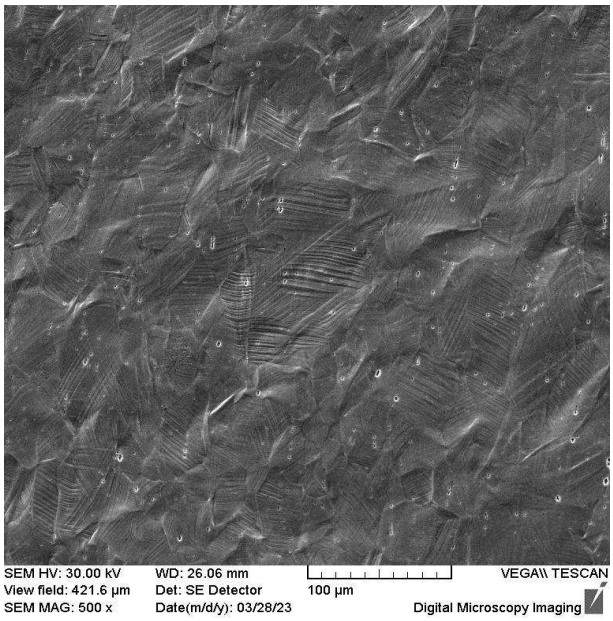

Fig. 24 *The surface of the AISI 304 specimen before the bending impact test – plastic deformation*

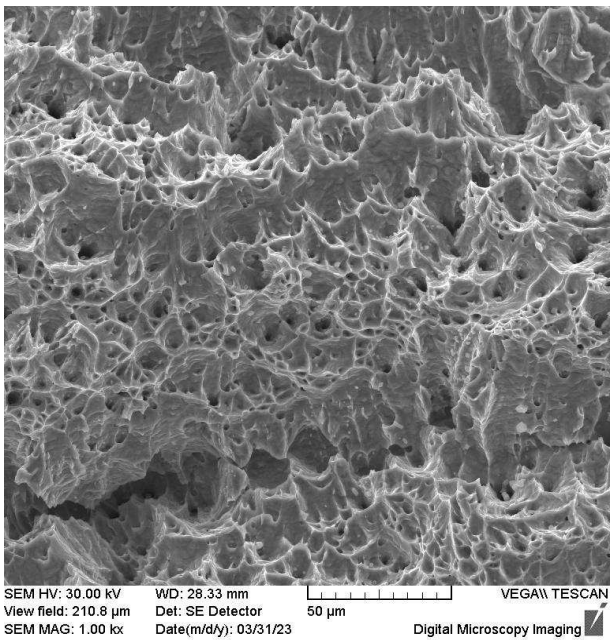

Fig. 25 *Fracture surface of AISI 304 after the bending impact test*

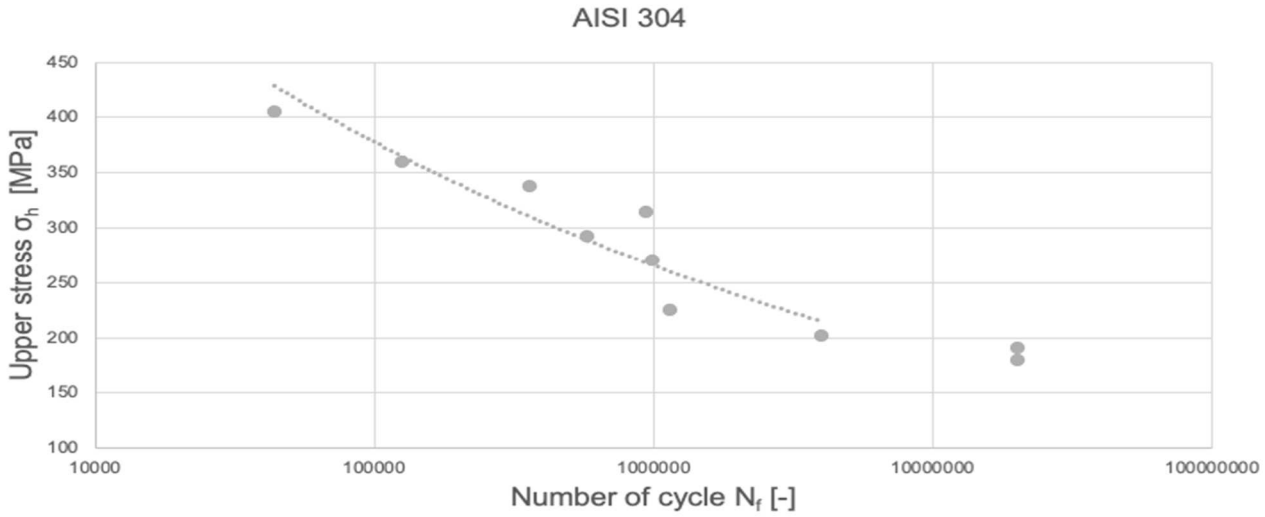

Fig. 26 *S-N curve - AISI 304*

From the SEM macroscopic evaluation of the fracture surface of AISI 304 austenitic steel after the fatigue test, it is possible to distinguish the location of the notch, the fatigue area, the transition area, and the static deformation area (Fig. 9). Fatigue cracks initiated in several locations, along the entire root of the notch. However, it is not possible to determine exactly what initiated the cracks. Intercrystalline cleavage facets, ductile striations, sulphides, and oxides, as well as secondary cracks, occur on fracture surfaces in the fatigue fracture zone.

The area of static failure was manifested by a ductile fracture with pit morphology.

Intercrystalline cleavage facets occur on the fracture surfaces in the fatigue fracture zone (Fig. 10a). Sulphidic and oxidic particles can be observed at the bottom of pits (Fig. 10b).

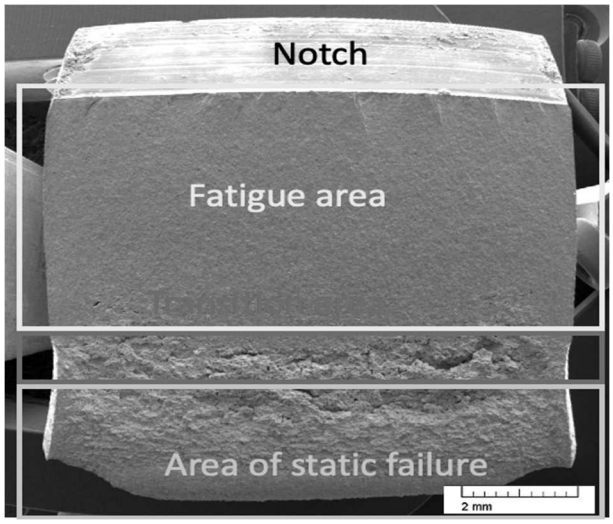

Fig. 27 *Fracture surface of AISI 304 after fatigue test*

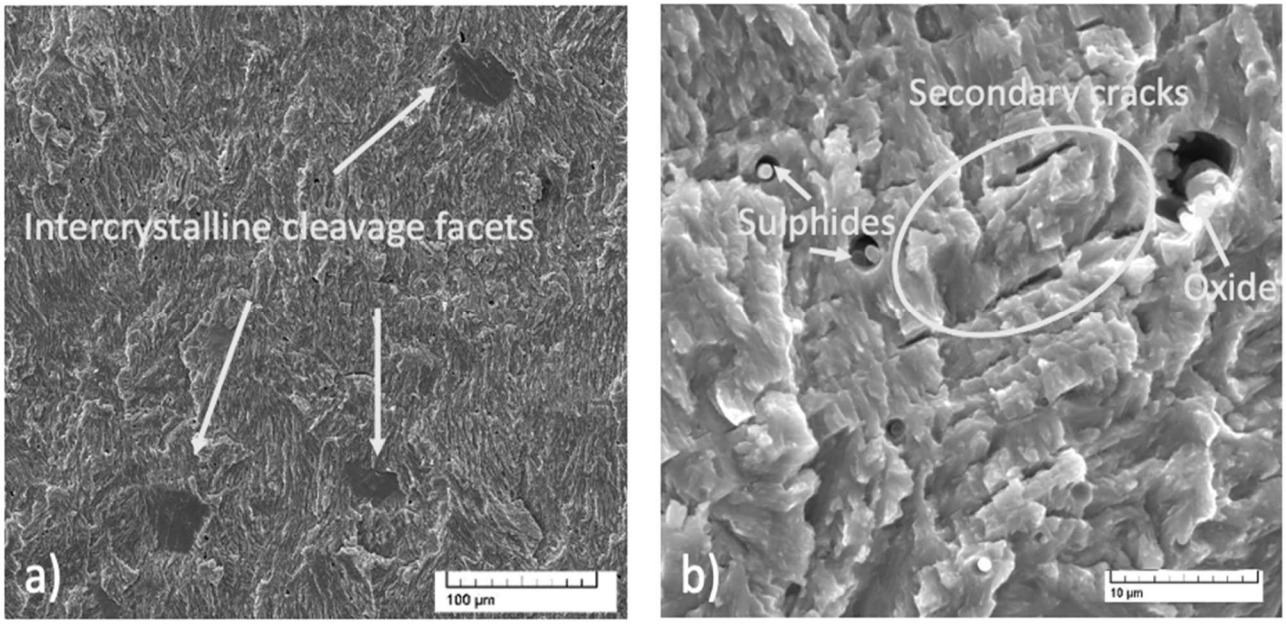

Fig. 28 *Areas of the fracture surface*

4 Conclusion

The whole experiment consisted of obtaining information on the chemical composition, microstructure, microhardness, and dynamic tests (bending impact test and Fatigue tests). The fracture surfaces were also evaluated after cyclic loading by three-point bending and after the bending impact test.

The chemical composition of AISI 304 austenitic steel differed in nickel, phosphorus, and sulfur content compared to the STN 17 240 standard. The microstructure of the steel was formed by polyhedral austenite grains of different sizes. The structure also included a large number of annealing twins and deformation martensite. The structure also contained a large number of non-metallic inclusions, which were identified by EDX analysis as manganese sulfides and oxides based on aluminum and silicon. Inclusions in metals are usually considered to be microstructural defects, that deteriorate mechanical properties or corrosion resistance.

The microhardness course has higher values, which may result in the amount of deformation martensite found in the steel structure. The carbon content of steel is unrelated to the amount of deformation martensite. Deformation martensite is formed when the austenitic grain deforms. The amount of strain martensite is influenced by the magnitude of the load (e.g. in rolling) and also by the condition after heat treatment. The amount of strain martensite affects the material properties. Higher microhardness is expected with higher amounts. After the bending impact test, all test specimens failed by ductile fracture with a typical pit morphology. Deep pits were observed on the fracture surface, which was formed after punctured test specimens, and it indicates a high energy of material failure. Sulfide particles were observed at the bottom of the pits, which form a so-called textured fracture, and due to them, the rolling direction, the linearity, and the deformation texture can be observed. By fractographic evaluation of the fracture surfaces, areas of crack initiation, transition area, as well as fatigue were recognized. It was possible to determine the initiation sites, from which the fatigue crack started, but it was not possible to determine where it initiated.

Acknowledgement

The research was supported by the Scientific Grant Agency of the Ministry of Education of Slovak Republic and Slovak Academy of Sciences, VEGA 01/0134/20, KEGA 004ŽU-4/2023, KEGA 016ŽU-4/2023, project APVV-20-0427 and project to support young researchers at UNIZA, the ID of project 12715.

References

[1] HAYAJNEH, M.T., ALMOMANI, M., AL-DARAGHMEH, M. (2019). Enhancement of the Corrosion Resistance of AISI 304 Stainless Steel by Nanocomposite Gelatin-Titanium Dioxide Coatings. In: *Manufacturing Technology*, Vol. 19, No. 5, pp. 759-766. ISSN 1213–2489

[2] ZATKALÍKOVÁ, V., MARKOVIČOVÁ, L., LIPTÁKOVÁ, T. A. VAŠKO, A. (2017). Corrosion Behavior of AISI 304 Stainless Steel in Aggressive Chloride Environment. In: *Manufacturing Technology*, Vol. 17, No. 4, pp. 639-643. ISSN 1213–2489

[3] ZATKALÍKOVÁ, V., MARKOVIČOVÁ, L., BELAN, J., LIPTÁKOVÁ, T. (2014). Variability of Local Corrosion Attack Morphology of AISI 316Ti Stainless Steel in Aggressive Chloride Environment. In: *Manufacturing Technology*, Vol. 14, No. 3, pp. 493-497. ISSN 1213–2489

[4] RODRÍGUEZ-MARTÍNEZ J.A., PESCI, R., RUSINEK, A. (2011). Experimental study on the martensitic transformation in AISI 304 steel sheets subjected to tension under wide ranges of strain rate at room temperature, In: *Materials Science and Engineering:* A, Vol. e 528, No. 18, pp. 5974-5982. ISSN 0921-5093

[5] BALUSAMY, T., SANKARA NARAYANAN, T.S.N., RAVICHANDRAN K, IL SONG PARK, MIN HO LEE. (2013). Influence of surface mechanical attrition treatment (SMAT) on the corrosion behavior of AISI 304 stainless steel, In: *Corrosion Science*, Vol. 74, pp. 332-344, ISSN 0010-938X

[6] BELYAKOV, A., SAKAI, T., MIURA, H. (2001). Microstructure and deformation behavior of sub microcrystalline 304 stainless steel produced by severe plastic deformation, In: *Materials Science and Engineering*: A, Vol. 319–321, pp. 867-871. ISSN 0921-5093

[7] NARAYANA MURTY, S.V.S., NAGESWARA RAO, B., KASHYAP, B.P. (2005). Identification of flow instabilities in the processing maps of AISI 304 stainless steel, In: *Journal of Materials Processing Technology*, Vol. 166, No. 2, pp. 268-278. ISSN 0924-013

[8] MILAD, M., ZREIBA, N., ELHALOUANI, F., BARADAI, C. (2008). The effect of cold work on structure and properties of AISI 304 stainless steel, In: *Journal of Materials Processing Technology,* Vol. 203, No. 1–3, pp. 80-85. ISSN 0924-0136

[9] MUKHOPADHYAY, C.K., JAYAKUMAR, T., KASIVISWANATHAN, K.V. (1995). Study of aging-induced α'-martensite formation in cold-worked AISI type 304 stainless steel using an acoustic emission technique. In: J Mater Sci 30, pp. 4556–4560. ISSN 1573-4803

[10] PALČEK, P., ORAVCOVÁ, M., CHALUPOVÁ, M., UHRÍČIK, M. (2016). The Usage of SEM for Fatigue Properties Evaluation of Austenitic Stainless Steel AISI 316L. In: *Manufacturing Technology*, Vol. 16, No. 5, pp. 1110-1115. ISSN 1213–2489

[11] UHRÍČIK, M., ORAVCOVÁ, M., PALČEK, P. AND CHALUPOVÁ, M. (2016). The Stress Detection and the Fatigue Lifetime of Stainless Steel during Three-Point Bending Cyclic Loading. In: *Manufacturing Technology*, Vol. 16, No. 5, pp. 1179-1182. ISSN 1213–2489

[12] ZÁVODSKÁ, D., GUAGLIANO, M., BOKŮVKA, O., TRŠKO, L. (2016). Effect of Shot Peening on the Fatigue Properties of 40NiCrMo7 steel. In: *Výrobná technológia*, Vol. 16, No. 1, pp. 295-299. ISSN 1213–2489

[13] DE VRIES, M.I., MASTENBROEK, A. (1977). SEM observations of dislocation substructures around fatigue cracks in Aisi type 304 stainless steel. In: *Metall Trans A 8*, pp. 1497–1499. ISSN 1073-5623

[14] YANG, L., ZHENGTONG, L., TINGCHAO, L., DALEI, L., JINSHENG, L., LIAW P.K., ZOU, Y. (2020). Effects of Surface Severe Plastic Deformation on the Mechanical Behavior of 304 Stainless Steel. In: *Metals*. Vol. 10, No. 6. ISSN 2075-4701

[15] XIE, S., WU, L., ZONGFEI, T., CHEN, H., ZHENMAO, C., UCHIMOTO, T., TAKAGI, T. (2018). Influence of Plastic Deformation and Fatigue Damage on Electromagnetic Properties of 304 Austenitic Stainless Steel. In: *IEEE Transactions on Magnetics*, Vol. 54, No. 8, pp. 1-10. ISSN 1941-0069

[16] WANG, JY-AN. (2020). Fracture toughness evaluation for thin-shell stainless steel weldment. In: *Theoretical and Applied Fracture Mechanics*, Vol. 106, pp. 102467. ISSN 0167-8442

[17] KARNATI, S., KHIABHANI, A., FLOOD, A., LIOU, F. W., NEWKIRK, J.W. (2018). Characterization of Impact Toughness of 304L Stainless Steel Fabricated through Laser Powder Bed Fusion Process. In: *Department of Mechanical and Aerospace Engineering*, Missouri University of Science and Technology, Rolla, MO 65409.

[18] ALHAJJI, E., M. (2016). Ductile and Brittle Fracture of 1018 Steel and 304 Stainless Steel Using Charpy Impact Test. In: *Department of Materials Science and Engineering*. MSE 355 Lab Report 201A.